


Article

Selective Functionalization of High-Resolution Cu₂O Nanopatterns via Galvanic Replacement for Highly Enhanced Gas Sensing Performance

Ju Ye Kim ^{1,2,†}, Soo-Yeon Cho ^{1,2,†} and Hee-Tae Jung ^{1,2,*} 

¹ Department of Chemical and Biomolecular Engineering (BK-21 Plus), Korea Advanced Institute of Science and Technology (KAIST), 291 Daehak-ro, Yuseong-gu, Daejeon 34141, Korea; juyekim@kaist.ac.kr (J.Y.K.); chosooyeon@kaist.ac.kr (S.-Y.C.)

² Korea Advanced Institute of Science and Technology (KAIST) Institute for NanoCentury, 291 Daehak-ro, Yuseong-gu, Daejeon 34141, Korea

* Correspondence: heetae@kaist.ac.kr; Tel.: +82-042-350-3931

† These authors contributed equally to this work.

Received: 21 November 2018; Accepted: 13 December 2018; Published: 15 December 2018



Abstract: Recently, high-resolution patterned metal oxide semiconductors (MOS) have gained considerable attention for enhanced gas sensing performance due to their polycrystalline nature, ultrasmall grain size (~5 nm), patternable properties, and high surface-to-volume ratio. Herein, we significantly enhanced the sensing performance of that patterned MOS by galvanic replacement, which allows for selective functionalization on ultrathin Cu₂O nanopatterns. Based on the reduction potential energy difference between the base channel material (Cu₂O) and the decorated metal ion (Pt²⁺), Pt could be selectively and precisely decorated onto the desired area of the Cu₂O nanochannel array. Overall, the Pt-decorated Cu₂O exhibited 11-fold higher NO₂ (100 ppm) sensing sensitivity as compared to the non-decorated sensing channel, the while the channel device with excessive Pt doping showed complete loss of sensing properties.

Keywords: gas sensor; nanopattern; chemical sensitization; galvanic replacement; p-type metal oxide; high-resolution

1. Introduction

Metal oxide semiconductors (MOSs) (e.g., n-type [1–5] and p-type [6–12]) are widely used as gas sensing materials due to their high sensitivity, large specific surface area, applicability to various gases (NO₂, CO₂, H₂, volatile organic compounds (VOCs), etc.), high electron mobility, and good chemical/thermal stability at high operating temperature [13–20]. Many approaches have been adopted to enhance the gas sensing performance of the MOS, including grain size refinement, increasing the surface area, reducing the interface area between the substrate and the device, and introduction of dopants and defects [1,18–22]. Doping with noble metals such as Pt [21,22], Pd [23], and Ag [2] has been widely used to enhance the sensing performance of the MOS by tuning the gas adsorption or diffusion properties. As sensitizers on the MOS surface, noble metals can induce electronic or chemical sensitization pathways [1,21]. Electronic sensitization occurs due to the electronic interaction between the semiconductor and the doped metal. When metal dopants undergo partial oxidation in air, their oxidation state of the metal additive can be changed into metallic state depending on the environment. This increases the depth of the electron-depleted charge layer due to electron extraction from the metal oxide, thereby changing the electronic state change of the MOS. The chemical sensitization represents a spill-over effect by activating target gas adsorption on the semiconductor surface [24]. The doped promoter facilitates target gas as active state, leading to

increases gas concentration on the channel surface. During the sensing process, the concentration of the adsorbed target gas is effectively increased by the promoter.

Recently, a patterned p-type polycrystalline MOS with an ultrathin and a high aspect ratio showed 5-fold enhanced gas sensing performance due to its ultra-small grains (~5 nm) and large surface-to-volume ratio [6,25]. One of the promising ways to improve the sensing properties is noble metal decoration on the MOS sensing channel. The conventional methods for metal functionalization include sputtering [2,23], thermal evaporation [3], electrospinning [21], and wet impregnation [22] in an aqueous solution. Since the evaporation technique does not allow for selective functionalization of the MOS channel with noble metals, undesired decoration of noble metals on the electrode and substrate can hinder effective control of the doping concentration and cause non-uniform deposition. Moreover, non-directional decoration can produce another dopant-connected channel that reduces the sensitivity of the MOS channel and causes malfunction of the sensing device. Thus, for reduced channel dimensions and higher resolution, more selective and direct functionalization is required [26].

In this study, we selectively functionalized a high-resolution p-type Cu_2O sensing channel with Pt nanoparticles by galvanic replacement in order to significantly enhance the gas sensing performance. High-resolution (10 nm scale) and high-aspect-ratio (~25) Cu_2O nanopatterns are fabricated via a unique lithographic technique with low-energy plasma bombardments. The unique morphological characteristics (resolution, aspect ratio, grain composition, fully exposed structure) of the Cu_2O nanopattern and the possibility of large-area fabrication make it the optimum nanostructure for the sensing channel of gas sensors. Galvanic replacement was employed to further enhance the gas sensing performance of the high-resolution Cu_2O nanopattern. This facile decoration process involves a chemical reaction between two materials with different reduction potentials [27–30]. Hence, selective functionalization on the target site is possible, and the size and the amount of the state of Cu_2O and to confirm the existence of Pt on the surface. Decorated dopants can be controlled by adjusting the precursor concentration and reaction conditions. The optimally functionalized nanochannel array ($\text{Cu}_2\text{O}/\text{Pt}$) shows 11-fold higher sensitivity as compared to the pristine Cu_2O array upon exposure to 100 ppm NO_2 gas (300 °C), because of electronic and chemical sensitization effects of the decorated Pt nanoparticles.

2. Materials and Methods

2.1. Cu_2O Nanopattern Fabrication

A polydimethylsiloxane (PDMS) mold was obtained by using a Si pre-patterned mask after curing a silicone elastomer mixture (Sylgard 184, 10:1 weight ratio of base to curing agent; Dow Corning, Midland, MI, USA). Polystyrene (18000 g/mol) solution in toluene was spin-coated (3000 rpm, 45 s) onto a SiO_2 -coated (200 nm) Si wafer to obtain a thin polystyrene (PS) film. The PS pre-pattern (500 nm width, 350 nm height) was created using capillary forces between PS and PDMS upon heating above the T_g (glass transition temperature, ~135 °C) in a vacuum oven. Then, the target metal (Cu, 25 nm thick) was uniformly deposited onto the PS pre-pattern by electron beam evaporation. By Ar ion bombardment at low energy (500 eV) with a wide angle distribution, the Cu thin layer was etched and emitted into the PS pre-patterned side wall to obtain a polycrystalline feature. After the PS residue was removed by oxygen reactive ion etching (RIE) under a low vacuum and O_2 (100 standard cubic centimeters per minute (sccm)) plasma environment, thermal oxidation was performed in a tubular furnace at 450 °C for 3 h to obtain a Cu_2O line channel.

2.2. Galvanic Reaction

To decorate Pt nanoparticles selectively onto the Cu_2O line pattern, 1 mL of 1 mM potassium tetrachloroplatinate (K_2PtCl_6 , Sigma Aldrich, Burlington, MA, USA), 1 mL of 1 mM hydrochloric acid (HCl, Sigma Aldrich), 5 mL of 20 mM sodium hydroxide powder (NaOH, Daejung), and 5 mL of 10 mM ascorbic acid (AA, Sigma Aldrich) were added to the Cu_2O line pattern substrate. This reaction

was performed at room temperature (RT) to control the reaction pace preventing over-loaded Pt. Then, the sample and solutions were injected into a 30 mL vial and agitated on a SK-300 benchtop shaker (90 rpm, Lab Companion, Daejeon, Korea). After each reaction, the substrate was cleaned with ethanol and DI water, and then dried under N₂.

2.3. Characterization

The surface morphology of the fabricated Cu₂O polycrystalline array and Pt-decorated line pattern was characterized by field-emission scanning electron microscopy (Magellan 400, Nova 230, ThermoFisher, Hillsboro, OR, USA) and energy-dispersive X-ray (EDS) spectroscopy (cmodel, manufacturer, city, xstae abbrev if USA, country). The electron beam energy was 5 kV and 10 kV for the EDS analysis. For the line depth and width profiling of the metal oxide pattern array, atomic force microscopy (AFM; XE-100, Park Systems, Suwon, Korea) was used. X-ray photoelectron spectroscopy (XPS, K-alpha, ThermoFisher, Hillsboro, OR, USA) analysis was conducted to verify the oxidation state of Cu₂O and to confirm the existence of Pt on the surface.

2.4. Sensor Fabrication and Measurement

To measure the resistance signal of the channel, 70-nm-thick Au electrodes with a predeposited 5-nm-thick Ti adhesion layer, as well as 100 μm spacing and width, were deposited the Cu₂O-Pt line pattern by e-beam evaporation using a customized SERS mask [31]. For saturation of oxygen gas on the substrate, air (400 sccm) was injected over 3 h at 260 °C into the sealed gas reaction chamber where the prepared metal oxide channel device was located. The external sources are used to heat sensing substrate. Heater module is right below the chamber plate. The size of the sealed gas sensing chamber was approximately 10 cm (width) × 5 cm (height) × 8 mm (depth). The resistance signals were displayed directly on a computer via a customized data acquisition module (34970A, Agilent, Santa Clara, CA, USA) to verify the gas sensitivity. NO₂ gas (100 ppm) was delivered into the sensing chamber every 10 min by a mass flow controller (MFC, 5850E, Brooks, Seattle, WA, USA). Air was used for observing the desorption properties.

3. Results and Discussion

3.1. Fabrication of Pt Decorated High-Resolution Cu₂O Nanochannel

The overall fabrication of the Pt-functionalized Cu₂O sensing channel (Cu₂O/Pt) is illustrated in Figure 1. First, a PS prepattern with 500 nm width and 350 nm height was formed on a Si wafer substrate on which SiO₂ was deposited via thermal pattern transfer using a PDMS mold (Figure 1a). By e-beam evaporation, a 25-nm-thick Cu nanofilm was uniformly deposited on the prepatterns (Figure 1b). The Cu layers were then etched such that they covered the side surfaces of the prepattern by using wide-angle distribution by a lower-energy plasma (500 eV, Ar⁺) bombardment process using ion-milling instruments. Bombardment of the Cu precursor layers with low-energy Ar⁺ plasma ruptures the Cu nanofilms to form 5-nm high-resolution grains that are sputtered over a wide area [32,33]. This leads to the formation of a polycrystalline Cu nanopattern with a high aspect ratio as a result of the attachment of the 5-nm Cu grains to the side wall of the PS prepatterns. After removing the polymer residue by oxygen RIE, ultra-high-resolution of the Cu line nanochannel remained (Figure 1d). To oxidize Cu into Cu₂O, the fabricated nanopattern was subjected to thermal annealing in a tubular furnace at 450 °C for 3 h in air and then cooled to RT (Figure 1e).

Since the galvanic reaction occurs only between target materials that have different reduction energy potentials, selective doping on the Cu₂O device channel can be possible without undesired deposition (e.g., on the substrate). Functionalized Pt can enhance the sensing performance of the Cu₂O channel due to the spill-over effect, i.e., easy dissociation of the adsorbed gas on the metal surface and subsequent migration into the metal oxide surface. Therefore, interparticle doping via galvanic replacement not only leads to an accessible contact distance so that gases can easily adsorbed

and desorbed, but also prevents the target gas from being captured by stray particles, which may hinder gas detection. Pt functionalization by the galvanic reaction was performed after synthesizing the Cu₂O nanopattern (Figure 1f). Since galvanic replacement generally results in a porous interior morphology [34], changing the exterior surface of the original material using another precursor in a strongly acidic environment induces fast reduction, and the reaction pathway can be controlled by precise adjustment of the solution pH [35]. To control the reaction time slowly and prevent collapse of the nanopattern structure by reducing the power of galvanic reaction moderate, a certain amount of sodium hydroxide (NaOH) solution was added. Under harsh acidic conditions, the synthesized Cu₂O channels were destroyed, resulting in rapid dissolution of Cu₂O. Generally, reduction by a galvanic reaction will lead to the formation of a hollow structure via oxidation of the inner metal [34]. When the Cu₂O sensing array is dispersed in an aqueous mixture solution which are Pt⁴⁺ precursor for functionalizing, H⁺ to initiate the galvanic reaction and NaOH salt for limiting the chemical reaction slowly maintaining the pH value around 5, electrons transfer from Cu₂O to Pt⁴⁺ and reduction of Pt⁴⁺ itself on Cu₂O surface occur at the same time. Since Pt has a higher reduction potential energy than does Cu₂O, Pt is preferentially reduced, so that Cu₂O is replaced with Pt on the surface [36]. It is well known that when the pH of the reaction solution increases, the reducing power of AA is enhanced [35].

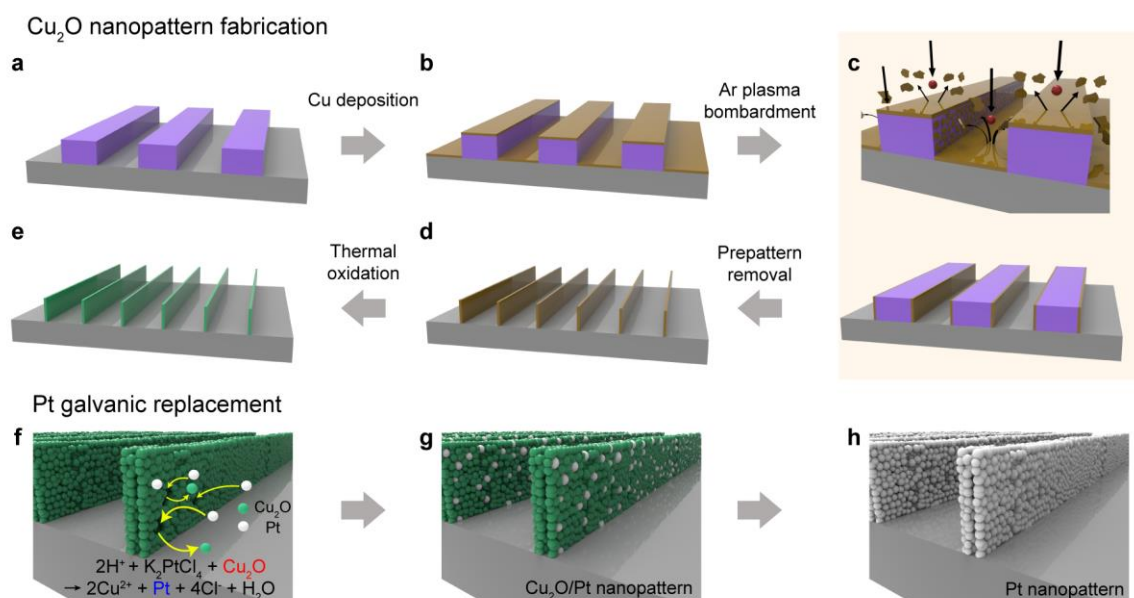


Figure 1. Schematic illustration of fabrication of Pt-functionalized high-resolution Cu₂O nanopattern. (a) The PS prepattern was transferred from the PDMS mold. (b) The target metal (Cu) was deposited onto the prepattern. (c) By low-energy plasma bombardments, the deposited metal was widely sputtered onto the side wall of the prepattern, resulting in polycrystalline Cu walls. (d) The prepattern residue was removed by RIE and (e) the ultra-thin Cu line pattern was oxidized by thermal annealing. (f) To functionalize the Cu₂O surface with Pt, the prepared channel was immersed in a Pt precursor solution. (g) The electrons were transferred from Cu₂O to Pt ions, resulting in the Pt-decorated Cu₂O nanopattern. (h) In case of an excessive galvanic reaction, the Cu₂O baseline channel was completely converted into Pt.

Therefore, by controlling the pH of the reaction solution with NaOH, we can adjust the galvanic reaction slowly, thus allowing both replacement and reduction without destroying the line pattern structure. After several hours of galvanic reaction at room temperature on a shaker, Pt ions were reduced into Pt particles onto the Cu₂O array surface, resulting in a Pt-decorated Cu₂O nanopattern (Figure 1g). To induce complete replacement, the experiment was performed in the same manner except for the addition of NaOH in the case of Pt nanowire array fabrication (Figure 1h). Under strongly acidic conditions without the addition of NaOH, the galvanic reaction predominates, resulting in

complete replacement of Cu₂O with Pt. To understand the reaction mechanism, schematic illustrations and supporting experimental results are presented in Figures S1 and S2.

3.2. Morphology, Elements, and Dimension Characterizations

To verify that selective Pt functionalization occurred only on the desired spot, scanning electron microscopy (SEM), energy-dispersive X-ray spectroscopy (EDS), and atomic force microscopy (AFM) were used (Figure 2). The pristine Cu₂O nanochannel with high resolution and high aspect ratio was well fabricated over a large area with a periodic spacing of 500 nm (Figure 2a). X-ray diffraction (XRD) shows that Cu nanopattern is successfully synthesized to Cu₂O nanopattern via thermal oxidation process (Figure S3). Photographs of the devices show that the Cu₂O nanopattern was fabricated over a large area (cm² scale) with excellent pattern fidelity (Figure S4). After 4 h of galvanic reaction, a part of the Cu₂O channel was successfully replaced with Pt nanoparticles without destruction or collapse of the high-aspect-ratio nanostructure. The yellow particles on the Cu₂O surface in Figure 2c were confirmed to be Pt via point EDS analysis by comparison that of the pristine Cu₂O. In addition, the overall distribution of the functionalized Pt was observed by TEM mapping analysis (Figure S5). Low-magnification SEM-EDS images clearly confirmed that the Pt nanoparticles existed only in the Cu₂O nanopatterns and there was no Pt in the substrate area between the Cu₂O channels (Figure 2c–f and Figure S6). These results revealed that the galvanic replacement selectively occurs at the target spots, i.e., the surface of the Cu₂O nanopatterns. With the reaction was carried out for a sufficient time under acidic conditions, replacement of Cu₂O with Pt was predominant, resulting in a pure Pt line pattern at the site of the Cu₂O pattern. To ensure complete reaction, the reaction was performed without the addition of NaOH (pH ~2). After a few hours, a Pt line pattern could be located at the original Cu₂O channel spots (Figure 2e), which supported the occurrence of the galvanic reaction, while EDS observations confirmed the presence of pure Pt wires (Figure 2f). AFM analysis revealed the feature dimensions of the Cu₂O nanopattern channel. The periodic Cu₂O lines were 15 nm in width and 320 nm in depth before the galvanic reaction; after Pt doping, the Cu₂O line nanopattern maintained its original features within the error range of the synthesis, thus indicating that the structure did not collapse during doping (Figure 1g–h). Overall, we fabricated high-resolution (15 nm) and high-aspect-ratio nanopatterns uniformly on a large area and achieved selective functionalization of Pt nanoparticles on the patterns. As discussed in a previous study [6], these nanopattern arrays have distinct advantages as a gas sensor: (1) polycrystalline feature with small grains; (2) low channel resistance caused by the large surface-to-volume ratio, which is derived from the ultrahigh resolution and high aspect ratio (~25). In addition, the noble metal acting as a sensitizer to enhance the gas sensing performance could be selectively decorated onto the surface of the ultrahigh-resolution nanopattern array by the galvanic replacement method.

3.3. Chemical Binding States of Pt/Cu₂O Nanochannel

To confirm the chemical binding state and oxidation state of the nanopattern channel, detailed surface elemental analysis was carried out by X-ray photoelectron spectroscopy (XPS). The obtained binding energy was calibrated with that of the C-C peak, 284.7 eV. Overlapping peaks were deconvoluted and identified using the Avantage Software program (Thermo Scientific™). As shown in Figure 3a, the metallic Cu nanopattern was completely oxidized and converted to Cu₂O upon thermal annealing. For Cu 2p photoelectron analysis, the binding energy range from 925 to 965 eV was scanned. The binding energy of metallic Cu was not detected in the Cu 2p spectrum, confirming that the Cu channel was fully oxidized into Cu₂O under the mild oxidation conditions. The high-resolution Cu 2p spectrum showed two main peaks at 933.18 eV and 952.98 eV, which could be assigned to the Cu²⁺ double peaks for Cu 2p_{3/2} and Cu 2p_{1/2} and three satellite peaks, respectively [37]. The two O 1s peaks represented the O²⁻ state (529.18 eV) from Cu₂O and the OH⁻ state (531.17 eV) from the adsorption of atmospheric oxygen on the surface [38]. The Cu 2p and O 1s peaks confirmed the formation of metal oxide (Cu₂O). Figure 3c shows the electron states of the Pt atoms in the nanopattern

channel. The doublet peaks at 74.24 eV and 71.19 eV corresponded to the binding energy of metallic Pt, and the binding energies at 78.2 eV and 75.3 eV were in agreement with Pt^{4+} which came from the binding between metal oxide and doped Pt [39]. During galvanic replacement, the Pt^{2+} ions penetrated the Cu_2O environment to form $\text{Cu}_2\text{O}/\text{Pt}$ species, ascribed to Pt^{4+} in the X-ray photoelectron spectrum. This Pt species binds to other Pt ions by accepting electrons from Cu_2O to form metallic Pt. From the Pt 4f spectral analysis, we can confirm that Pt^{2+} in the galvanic reaction solution (PtCl_4^{2-}) is successfully reduced to Pt metal without remaining in the ionic state on the Cu_2O surface.

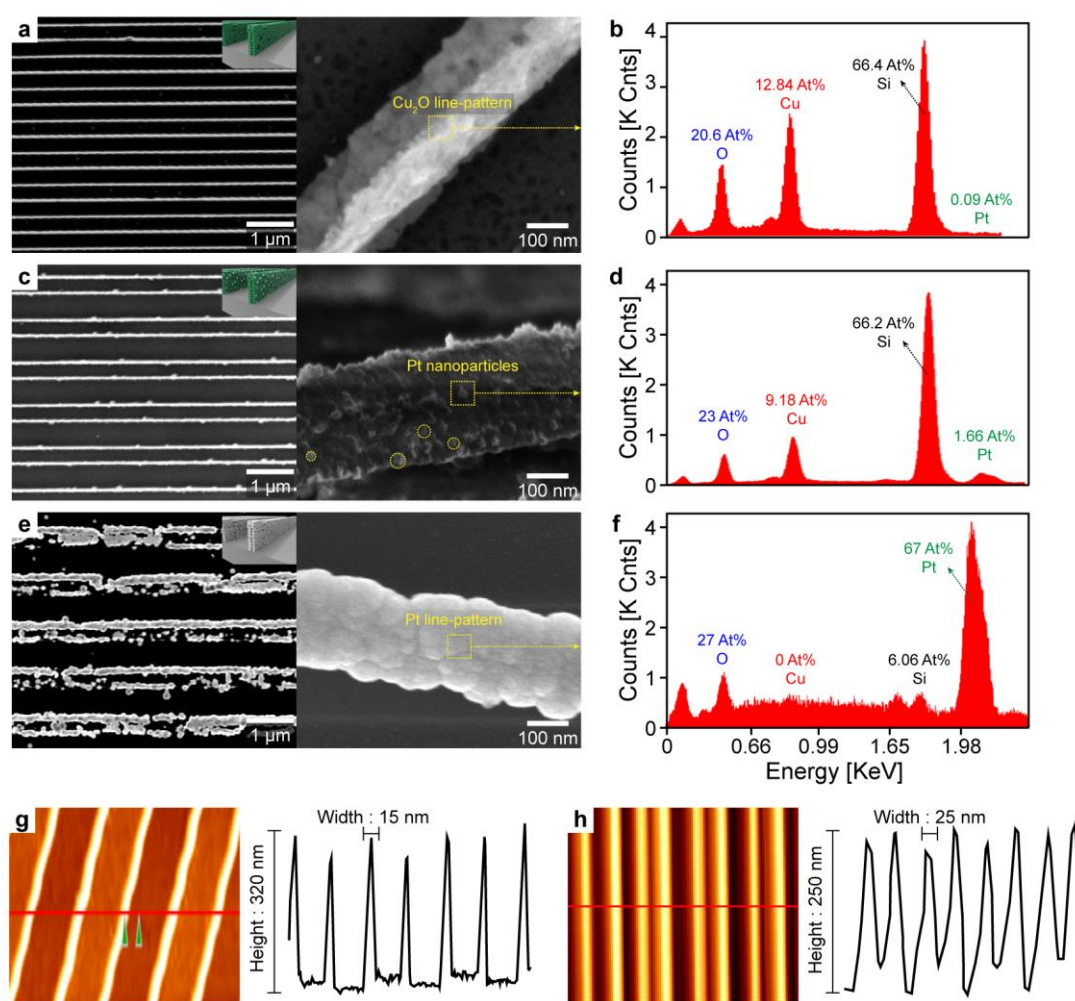


Figure 2. Characterization of fabricated Cu_2O , $\text{Pt}/\text{Cu}_2\text{O}$, and Pt sensing channel. SEM image of the fabricated pattern array for (a) pristine Cu_2O , (c) optimized Pt-doped Cu_2O , and (e) completely reacted Pt. (b–f) EDS point analysis of each channel. (g–h) AFM depth and width profiles show ultrathin line channel and no disruption of the pattern after Pt doping.

The synthesized ultrathin $\text{Pt}/\text{Cu}_2\text{O}$ nanopattern exhibited 11-fold higher sensitivity than did the pristine Cu_2O nanopattern. To determine the feasibility of using the $\text{Cu}_2\text{O}/\text{Pt}$ nanopattern as an electronic sensing channel, the baseline resistances and noise level of the channel were measured during $300\text{ }^\circ\text{C}$ operation (Figure 4a). The channel resistance of the pristine Cu_2O sensor was $24\text{ M}\Omega$, which increased, and approaching $\sim 45\text{ M}\Omega$ upon Pt nanoparticle decoration; a resistance level of tens of $\text{M}\Omega$ is within the optimal range for MOS-based gas sensors. The increase in the channel resistance was due to the formation of a depletion layer on the Cu_2O channel because of electron transfer from the decorated Pt nanoparticles. In addition, the noise from the $\text{Cu}_2\text{O}/\text{Pt}$ channel increased from 0.88% to 4.59% of the baseline resistance. However, the Pt nanopattern obtained by the excessive galvanic reaction showed a significantly low resistance (tens of Ω) with an ultra-low noise level due to

the metallic conductivity of the Pt nanopattern channel. To investigate the effects of Pt nanoparticle decoration on the sensing characteristics of the Cu₂O nanopattern, a sensing device was fabricated with integration of a nanopattern channel (Cu₂O, Cu₂O/Pt, Pt) and two-terminal resistor type electrodes. A constant bias from 0.5 to 1.5 V was automatically applied to the two-probe electrode, and the electrical resistance of each channel was recorded as a sensing signal by a data acquisition module (Agilent 34970A). The sensing devices were simultaneously loaded on a home-made gas sensing chamber, and the sensing signals from each device were measured with multi-channel sensing systems.

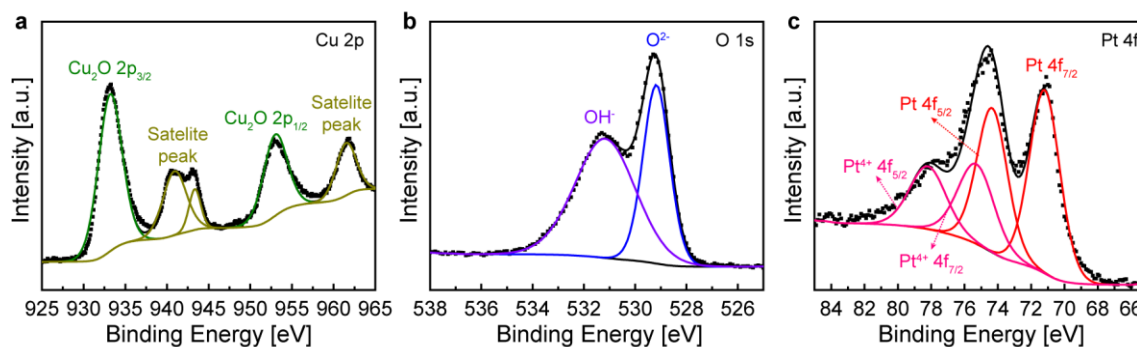


Figure 3. X-ray photoelectron spectra of Cu₂O/Pt nanopattern. High-resolution elemental spectra of (a) Cu 2p, (b) O 1s, and (c) Pt 4f.

3.4. NO₂ Sensing Performances and Mechanism

Details of the in-house fabricated gas delivery system are provided in the Supporting Information (Figure S7) [40]. Figure 4b shows the responses of the Cu₂O, Cu₂O/Pt, and Pt nanopatterns toward 100 ppm NO₂ at 300 °C. Gas response is defined as R_a/R_g , where R_a and R_g are the resistances of the sensor in air and in the target gas, respectively. The Cu₂O/Pt nanopattern exhibited a markedly higher sensitivity upon exposure to NO₂ ($R_a/R_g = 11$) than did the pristine Cu₂O nanopattern ($R_a/R_g = 1$), which was attributed to the effect of the noble metal (Pt) nanoparticle decoration. For the Pt nanopattern obtained by the excessive galvanic replacement reaction, NO₂ detection was not observed due to the perfect metallic properties of the nanopattern. To further investigate the high sensitivity of the Cu₂O/Pt nanopattern sensor, real-time sensing response to single ppm of NO₂ (1 to 4 ppm) is measured (Figure 4c). It is clearly seen that Cu₂O/Pt nanopattern sensors show significant responses to single ppm NO₂ with distinguishable signal resolutions. Figure 4d further demonstrates that the Cu₂O/Pt nanopattern sensors show linear response variations to single ppm NO₂ (1–4 ppm) with significant repose amplitudes ($(\Delta R/R_b)_{\max}$) which was comparable value with other previous works (Table S1). Here, R_b and ΔR represent the baseline resistance of the sensor exposed to dry air and the change in resistance after exposure to NO₂, respectively. Thus, selective functionalization of the Cu₂O channel by galvanic replacement had a significant impact on the enhancement of the gas sensing performance. The response/recovery time ($\tau_{90\%}$, time taken to reach the 90% of the minimum resistance level) of the sensors for NO₂ is shown in Figure S8. Moreover, functionalized Cu₂O/Pt doesn't change the selectivity characterization comparing that of Cu₂O (see the Figure S9 which shows similar response selectivity comparing that of Cu₂O [6] among various gases). In addition, long-term stability test of the Cu₂O/Pt nanopattern sensor was conducted showing high-stability of synthesized catalyst (Figure S10). The highly enhanced gas sensing performance of Cu₂O with the Pt galvanic reaction could be explained via two mechanisms: electronic sensitization (ES) [24,41,42] and chemical sensitization (CS) [24,43,44]. The detailed enhancement mechanisms are shown in Figure 4e–g. First, the decorated Pt nanoparticles played an ES role during the sensing process. When exposed to air, each Pt nanoparticle consisting of Pt and Pt⁴⁺ forms a redox electrode Pt⁴⁺/Pt⁰. To achieve electronic equilibrium with the Pt nanoparticles, the Fermi level of Cu₂O will be shifted and pinned at the Pt⁴⁺/Pt⁰ electrode potential, which produces an electron-depleted space charge region and decreases the charge (hole) accumulation layer (HAL) (Figure 4e). This eventually leads to an increase in the resistance of the

pristine $\text{Cu}_2\text{O}/\text{Pt}$ in air. Second, the functionalized Pt nanoparticles also play an important role via the CS mechanism because of the spillover effect. For the pristine Cu_2O nanopattern, the adsorbed oxygen ions (O^- , O^{2-}) localize the electrons, which leads to an increase in the concentration of holes in the surface layers. Upon exposure to NO_2 , the adsorbed NO_2 ions (NO_2^-) further localize the electrons of Cu_2O , thus increasing the HAL thickness and decreasing the resistance of the sensors (Figure 4f–g). In the case of $\text{Cu}_2\text{O}/\text{Pt}$, significantly larger amounts of NO_2 can be adsorbed onto Cu_2O via the spill-over effect [43,44] due to the high catalytic activity of the Pt nanoparticles (Figure 4f). Thus, the high-resolution Cu_2O nanopattern is selectively functionalized with Pt nanoparticles via the galvanic replacement reaction, and the gas sensing performance is significantly improved via both the ES and CS mechanisms.

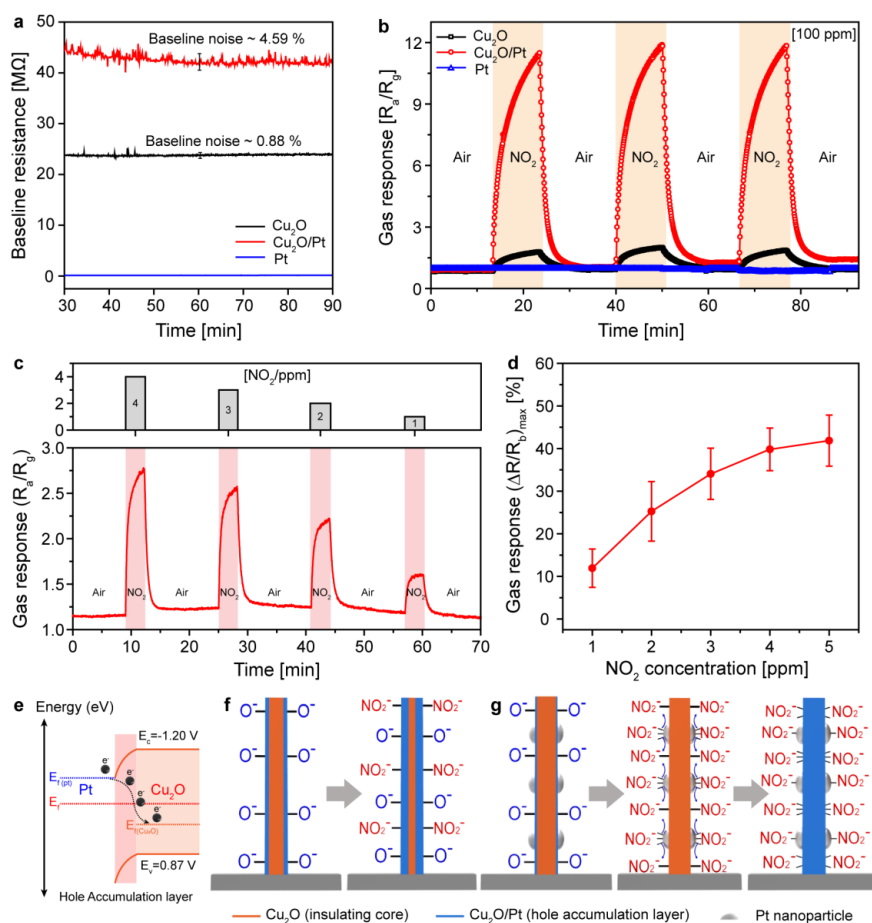


Figure 4. Device characteristics and gas sensing performance of the Cu_2O , $\text{Cu}_2\text{O}/\text{Pt}$, and Pt nanopattern sensors. (a) Baseline resistance and noise of the Cu_2O , $\text{Cu}_2\text{O}/\text{Pt}$, and Pt nanopattern. (b) Real-time NO_2 (100 ppm) sensing performance of the Cu_2O , $\text{Cu}_2\text{O}/\text{Pt}$, and Pt nanopattern sensors. (c) Real-time response behavior of the $\text{Cu}_2\text{O}/\text{Pt}$ nanopattern sensor to low concentration NO_2 (1 to 4 ppm). (d) Maximum response amplitudes of the $\text{Cu}_2\text{O}/\text{Pt}$ nanopattern sensor (three sensors) to low concentration NO_2 . (e) Band diagram scheme of $\text{Cu}_2\text{O}/\text{Pt}$ to elucidate electronic sensitization (ES). Schematic illustrations of chemical sensing mechanism of (f) Cu_2O and (g) $\text{Cu}_2\text{O}/\text{Pt}$ nanopattern with chemical sensitization (CS) of spill-over effect by Pt nanoparticles.

4. Conclusions

In conclusion, an ultrahigh resolution array, i.e., a thin, polycrystalline, and high-aspect-ratio p-type sensing channel array (Cu_2O) was selectively functionalized with Pt via galvanic replacement. Herein, by using a galvanic reaction which involves a chemical reaction between two materials, we achieved selective doping of Pt onto the surface of the ultrahigh-resolution nanopattern array.

We successfully fabricated an ultrathin nanopattern array with a high surface-to-volume ratio over a large area by our unique lithography technique (low-energy plasma bombardment [23]) and showed enhancement of the sensing performance after selective Pt functionalization through the galvanic replacement reaction. The sensor with Pt-functionalized Cu₂O showed a 11-fold increase in the gas response (R_a/R_g) to the bare Cu₂O channel when exposed on 100 ppm NO₂. The role of the functionalized Pt particles was suggested in terms of both ES and CS mechanisms. Using the selectively Pt-decorated high-resolution Cu₂O array obtained via galvanic replacement, we could achieve significant enhancement of the NO₂ sensing performance.

Supplementary Materials: The following are available online at <http://www.mdpi.com/1424-8220/18/12/4438/s1>, Figure S1: schematic illustrations of expected galvanic reaction process, Figure S2: scanning electron microscope (SEM) observations depending on various reaction condition, Figure S3: XRD spectrum of the Cu₂O nanopattern before and after thermal oxidation, Figure S4: photo and SEM image of the Cu₂O nanopattern sensors, Figure S5: elemental distribution analysis by transmission electron microscopy (TEM) - energy dispersive X-ray spectroscopy (EDS), Figure S6: the composition analysis of over-galvanic reacted sample to confirm a selective decoration property of galvanic reaction, Figure S7: schematic of the overall gas delivery system, Figure S8: response and recovery time of the Cu₂O/Pt nanopattern sensors to 1 to 4 ppm NO₂, Figure S9: selectivity characterization of the Cu₂O/Pt nanopattern sensor, Figure S10: long-term stability of the Cu₂O/Pt nanopattern sensor. Table S1: NO₂ gas sensing performance comparison based on CuO or Cu₂O materials.

Author Contributions: Conceptualization, validation, writing—review & editing, and writing—original draft preparation, funding acquisition, resources, project administration, J.Y.K. and S.-Y.C.; methodology, investigation, J.Y.K.; data curation, visualization, formal analysis, S.-Y.C.; supervision, and writing—review & editing, H.-T.J.

Funding: This research was supported by a National Research Foundation of Korea (NRF) grant funded by the Ministry of Science, ICT and Future Planning, Korea (NRF-2018R1A2B3008658) and a Global Frontier grant funded by the Center for Advanced Soft Electronics under the Global Frontier Research Program of the Ministry of Science, ICT and Future Planning, Korea (MSIP, NRF-2012M3A6A5055744).

Conflicts of Interest: The authors declare no conflict of interest.

References

1. Velmathi, G.; Mohan, S.; Henry, R. Analysis of factors for improving functionality of tin oxide gas sensor. *IETE Tech. Rev.* **2016**, *33*, 122–129. [[CrossRef](#)]
2. Hwang, I.-S.; Choi, J.-K.; Woo, H.-S.; Kim, S.-J.; Jung, S.-Y.; Seong, T.-Y.; Kim, I.-D.; Lee, J.-H. Facile control of C₂H₅OH sensing characteristics by decorating discrete Ag nanoclusters on SnO₂ nanowire networks. *ACS Appl. Mater. Interfaces* **2011**, *3*, 3140–3145. [[CrossRef](#)] [[PubMed](#)]
3. Shimizu, Y.; Matsunaga, N.; Hyodo, T.; Egashira, M. Improvement of SO₂ sensing properties of WO₃ by noble metal loading. *Sens. Actuators B Chem.* **2001**, *77*, 35–40. [[CrossRef](#)]
4. Chang, Y.-E.; Youn, D.-Y.; Ankonina, G.; Yang, D.-J.; Kim, H.-G.; Rothschild, A.; Kim, I.-D. Fabrication and gas sensing properties of hollow SnO₂ hemispheres. *Chem. Commun.* **2009**, *27*, 4019–4021. [[CrossRef](#)]
5. Ahn, M.-W.; Park, K.-S.; Heo, J.-H.; Park, J.-G.; Kim, D.-W.; Choi, K.J.; Lee, J.-H.; Hong, S.-H. Gas sensing properties of defect-controlled ZnO-nanowire gas sensor. *Appl. Phys. Lett.* **2008**, *93*, 263103. [[CrossRef](#)]
6. Cho, S.-Y.; Yoo, H.-W.; Kim, J.Y.; Jung, W.-B.; Jin, M.L.; Kim, J.-S.; Jeon, H.-J.; Jung, H.-T. High-resolution p-type metal oxide semiconductor nanowire array as an ultrasensitive sensor for volatile organic compounds. *Nano Lett.* **2016**, *16*, 4508–4515. [[CrossRef](#)]
7. Kim, H.-J.; Lee, J.-H. Highly sensitive and selective gas sensors using p-type oxide semiconductors: Overview. *Sens. Actuators B Chem.* **2014**, *192*, 607–627. [[CrossRef](#)]
8. Thirumalairajan, S.; Girija, K.; Mastelaro, V.R.; Ponpandian, N. Surface morphology-dependent room-temperature LaFeO₃ nanostructure thin films as selective NO₂ gas sensor prepared by radio frequency magnetron sputtering. *ACS Appl. Mater. Interfaces* **2014**, *6*, 13917–13927. [[CrossRef](#)]
9. Joshi, N.; Silva, L.F.D.; Jadhav, H.; M'Peko, J.-C.; Torres, B.B.M.; Aguir, K.; Mastelaro, V.R., Jr.; Oliveira, N.O. One-step approach for preparing ozone gas sensors based on hierarchical NiCo₂O₄ structures. *RSC Adv.* **2016**, *6*, 92655–92662. [[CrossRef](#)]
10. Joshi, N.; Silva, L.F.D.; Jadhav, H.S.; Shimizu, F.M.; Suman, P.H.; M'Peko, J.-C.; Orlandi, M.O.; Seo, J.G.; Mastelaro, V.R., Jr.; Oliveira, N.O. Yolk-shelled ZnCo₂O₄ microspheres: Surface properties and gas sensing application. *Sens. Actuators B* **2018**, *257*, 906–915. [[CrossRef](#)]

11. Hu, J.; Zou, C.; Su, Y.; Li, M.; Han, Y.; Kong, E.S.-W.; Yang, Z.; Zhang, Y. An ultrasensitive NO₂ gas sensor based on a hierarchical Cu₂O/CuO mesocrystal nanoflower. *J. Mater. Chem. A* **2018**, *6*, 17120–17131. [[CrossRef](#)]
12. Hübner, M.; Simion, C.E.; Tomescu-Stănoiu, A.; Pokhrel, S.; Bârsan, N.; Weimar, U. Influence of humidity on CO sensing with p-type CuO thick film gas sensors. *Sens. Actuators B* **2011**, *153*, 347–353. [[CrossRef](#)]
13. Yoo, H.-W.; Cho, S.-Y.; Jeon, H.-J.; Jung, H.-T. Well-defined and high resolution Pt nanowire arrays for a high performance hydrogen sensor by a surface scattering phenomenon. *Anal. Chem.* **2015**, *87*, 1480–1484. [[CrossRef](#)] [[PubMed](#)]
14. Zhang, J.; Qin, Z.; Zeng, D.; Xie, C. Metal-oxide-semiconductor based gas sensors: Screening, preparation, and integration. *Phys. Chem. Chem. Phys.* **2017**, *19*, 6313–6329. [[CrossRef](#)] [[PubMed](#)]
15. Wang, C.; Yin, L.; Zhang, L.; Xiang, D.; Gao, R. Metal oxide gas sensors: Sensitivity and influencing factors. *Sensors* **2010**, *10*, 2088–2106. [[CrossRef](#)] [[PubMed](#)]
16. Miller, D.R.; Akbar, S.A.; Morris, P.A. Nanoscale metal oxide-based heterojunctions for gas sensing: A review. *Sens. Actuators B Chem.* **2014**, *204*, 250–272. [[CrossRef](#)]
17. Franke, M.E.; Koplín, T.J.; Simon, U. Metal and metal oxide nanoparticles in chemiresistors: Does the nanoscale matter? *Small* **2006**, *2*, 36–50. [[CrossRef](#)] [[PubMed](#)]
18. Liu, X.; Ma, T.; Pinna, N.; Zhang, J. Two-dimensional nanostructured materials for gas sensing. *Adv. Funct. Mater.* **2017**, *27*, 1702168. [[CrossRef](#)]
19. Joshi, N.; Hayasaka, T.; Liu, Y.; Liu, H., Jr.; Oliveira, N.O.; Lin, L. A review on chemiresistive room temperature gas sensors based on metal oxide nanostructures, graphene and 2D transition metal dichalcogenides. *Microchim. Acta* **2018**, *185*, 213. [[CrossRef](#)]
20. Zhang, J.; Liu, X.; Neri, G.; Pinna, N. Nanostructured materials for room-temperature gas sensors. *Adv. Mater.* **2016**, *28*, 795–831. [[CrossRef](#)]
21. Fu, J.; Zhao, C.; Zhang, J.; Peng, Y.; Xie, E. Enhanced gas sensing performance of electrospun Pt-functionalized NiO nanotubes with chemical and electronic sensitization. *ACS Appl. Mater. Interfaces* **2013**, *5*, 7410–7416. [[CrossRef](#)] [[PubMed](#)]
22. Gou, X.; Wang, G.; Yang, J.; Park, J.; Wexler, D. Chemical synthesis, characterization and gas sensing performance of copper oxide nanoribbons. *J. Mater. Chem.* **2008**, *18*, 965–969. [[CrossRef](#)]
23. Lu, Y.; Li, J.; Han, J.; Ng, H.-T.; Binder, C.; Partridge, C.; Meyyappan, M. Room temperature methane detection using palladium loaded single-walled carbon nanotube sensors. *Chem. Phys. Lett.* **2004**, *391*, 344–348. [[CrossRef](#)]
24. Yamazoe, N. New Approaches for improving semiconductor gas sensors. *Sens. Actuators B Chem.* **1991**, *5*, 7–19. [[CrossRef](#)]
25. Jeon, H.-J.; Kim, K.H.; Baek, Y.-K.; Kim, D.W.; Jung, H.-T. New top-down approach for fabricating high-aspect-ratio complex nanostructures with 10 nm scale features. *Nano Lett.* **2010**, *10*, 3604–3610. [[CrossRef](#)] [[PubMed](#)]
26. Shen, G.; Chen, P.-C.; Ryu, K.; Zhou, C. Devices and chemical sensing applications of metal oxide nanowires. *J. Mater. Chem.* **2009**, *19*, 828–839. [[CrossRef](#)]
27. Jang, H.-J.; Hong, S.; Ham, S.; Shuford, K.L.; Park, S. Site-specific growth of a Pt shell on Au nanoplates: Tailoring their surface plasmonic behavior. *Nanoscale* **2014**, *6*, 7339–7345. [[CrossRef](#)]
28. Seo, D.; Song, H. Asymmetric hollow nanorod formation through a partial galvanic replacement reaction. *J. Am. Chem. Soc.* **2009**, *131*, 18210–18211. [[CrossRef](#)]
29. Pradhan, M.; Chowdhury, J.; Sarkar, S.; Sinha, A.K.; Pal, T. Hierarchical gold flower with sharp tips from controlled galvanic replacement reaction for high surface enhanced Raman scattering Activity. *J. Phys. Chem. C* **2012**, *116*, 24301–24313. [[CrossRef](#)]
30. Zhang, W.; Rahmani, M.; Niu, W.; Ravaine, S.; Hong, M.; Lu, X. Tuning interior nanogaps of double-shelled Au/Ag nanoboxes for surface-enhanced Raman scattering. *Sci. Rep.* **2015**, *5*, 8382. [[CrossRef](#)]
31. Cho, S.-Y.; Kim, S.J.; Lee, Y.; Kim, J.-S.; Jung, W.-B.; Yoo, H.-W.; Kim, J.; Jung, H.-T. highly enhanced gas adsorption properties in vertically aligned MoS₂ layers. *ACS Nano* **2015**, *9*, 9314–9321. [[CrossRef](#)] [[PubMed](#)]
32. Cho, S.-Y.; Jeon, H.-J.; Yoo, H.-W.; Cho, K.M.; Jung, W.-B.; Kim, J.-S.; Jung, H.-T. Highly enhanced fluorescence signals of quantum dot–polymer composite arrays formed by hybridization of ultrathin plasmonic Au nanowalls. *Nano Lett.* **2015**, *15*, 7273–7280. [[CrossRef](#)] [[PubMed](#)]

33. Cho, S.-Y.; Jeon, H.-J.; Kim, J.-S.; Ok, J.M.; Jung, H.-T. Hierarchical ordering of quantum dots and liquid with tunable super-periodicity into high aspect ratio moiré superlattice structure. *Adv. Funct. Mater.* **2014**, *24*, 6939–6947. [[CrossRef](#)]
34. Zhang, W.; Yang, J.; Lu, X. Tailoring galvanic replacement reaction for the preparation of Pt/Ag bimetallic hollow nanostructures with controlled number of voids. *ACS Nano* **2012**, *6*, 7397–7405. [[CrossRef](#)] [[PubMed](#)]
35. Yang, Y.; Liu, J.; Fu, Z.-W.; Qin, D. Galvanic replacement-free deposition of Au on Ag for core-shell nanocubes with enhanced chemical stability and SERS activity. *J. Am. Chem. Soc.* **2014**, *136*, 8153–8156. [[CrossRef](#)] [[PubMed](#)]
36. Li, Q.; Xu, P.; Zhang, B.; Wu, G.; Zhao, H.; Fu, E.; Wang, H.-L. Self-supported Pt nanoclusters via galvanic replacement from Cu₂O nanocubes as efficient electrocatalysts. *Nanoscale* **2013**, *5*, 7397. [[CrossRef](#)] [[PubMed](#)]
37. Zhu, H.; Du, M.; Yu, D.L.; Wang, Y.; Wang, L.; Zou, M.; Zhang, M.; Fu, Y.Q. A new strategy for the surface-free-energy-distribution induced selective growth and controlled formation of Cu₂O-Au hierarchical heterostructures with a series of morphological evolutions. *J. Mater. Chem. A* **2013**, *1*, 919–929. [[CrossRef](#)]
38. Ji, R.; Sun, W.; Chu, Y. One-step hydrothermal synthesis of Ag/Cu₂O heterogeneous nanostructure over Cu foil and their SERS applications. *RSC Adv.* **2014**, *4*, 6055–6059. [[CrossRef](#)]
39. Murata, N.; Suzuki, T.; Kobayashi, M.; Togoh, F.; Asakura, K. Characterization of Pt-doped SnO₂ catalyst for a high-performance micro gas sensor. *Phys. Chem. Chem. Phys.* **2013**, *15*, 17938–17946. [[CrossRef](#)]
40. Cho, S.-Y.; Lee, Y.; Koh, H.-J.; Jung, H.; Kim, J.-S.; Yoo, H.-W.; Kim, J.; Jung, H.-T. Superior chemical sensing performance of black phosphorus: comparison with MoS₂ and graphene. *Adv. Mater.* **2016**, *28*, 7020–7028. [[CrossRef](#)]
41. Chen, D.; Liu, Z.; Guo, Z.; Yan, W.; Xin, Y. Enhancing light harvesting and charge separation of Cu₂O photocathodes with spatially separated noble-metal cocatalysts towards highly efficient water splitting. *J. Mater. Chem. A* **2018**, *6*, 20393–20401. [[CrossRef](#)]
42. Cao, D.; Wang, C.; Zheng, F.; Dong, W.; Fang, L.; Shen, M. High-efficiency ferroelectric-film solar cells with an n-type Cu₂O cathode buffer layer. *Nano Lett.* **2012**, *12*, 2803–2809. [[CrossRef](#)] [[PubMed](#)]
43. Wang, W.-J.; Liang, J.-R.; Li, C.-Q.; Yan, W.-J.; Hu, M. Room temperature NO₂ gas sensing of Au-loaded tungsten oxide nanowires/porous silicon hybrid structure. *Chin. Phys. B* **2015**, *25*, 028102. [[CrossRef](#)]
44. Mane, A.A.; Moholkar, A.V. Palladium (Pd) sensitized molybdenum trioxide (MoO₃) nanobelts for nitrogen dioxide (NO₂) gas detection. *Solid-State Electron.* **2018**, *139*, 21–30. [[CrossRef](#)]



© 2018 by the authors. Licensee MDPI, Basel, Switzerland. This article is an open access article distributed under the terms and conditions of the Creative Commons Attribution (CC BY) license (<http://creativecommons.org/licenses/by/4.0/>).